Atmospheric
Chemistry
and Physics
Discussions

1
2 **Tropospheric warming over the North Indian Ocean caused by the South Asian anthropogenic aerosols: possible implications**

3

4 Suvarna Fadnavis[1*], Prashant Chavan[1], Akash Joshi[2], Sunil Sonbawne[1], Asutosh Acharya[3],
5 Panuganti C S. Devara[4], Alexandru Rap[5], Rolf Müller[6]

6 [1]Indian Institute of Tropical meteorology, MoES, Pune, India

7 [2]Indian Institute of Technology, Kharagpur, India

8 [3]Indian Institute of Technology, Bhubneshwar, India

9 [4]Centre of Excellence in ACOAST/ACESH, Amity University Haryana (AUH), Gurugram
10 122413, India

11 [5]School of Earth and Environment, University of Leeds, Leeds, United Kingdom

12 [6]Forschungszentrum Jülich GmbH, IEK-7, Jülich, Germany

13 Corresponding author: Suvarna Fadnavis

14 Corresponding author email: suvarna@tropmet.res.in

15

16

17 **Abstract**

18 Atmospheric concentrations of South Asian anthropogenic aerosols and their transport play a

19 key role in the regional hydrological cycle. Here, we use the ECHAM6-HAMMOZ

20 chemistry-climate model to show the structure and implications of the transport pathways of

21 these aerosols during spring. Our simulations indicate that large amounts of anthropogenic

22 aerosols are transported from South Asia to the North Indian Ocean (the Arabian Sea and

23 North Bay of Bengal). These aerosols are then lifted into the upper troposphere and lower

24 stratosphere (UTLS) by the convection over the Arabian Sea and Bay of Bengal. In the

25 UTLS, they are further transported to the southern hemisphere (30-40°S) and downward into

26 the troposphere by the secondary circulation induced by the aerosol changes. The

27 carbonaceous aerosols are also transported to the Arctic and Antarctic producing local

28 heating ($0.002 – 0.05$ K d^{-1}).

29   The presence of anthropogenic aerosols causes negative radiative forcing (RF) at the TOA (-

30   0.90±0.089 W m^{-2}) and surface (-5.87±0.31 W m^{-2}) and atmospheric warming (+4.96±0.24 W

31   m^{-2}) over South Asia (60° E - 90° E, 8° N - 23° N), except over the Indo-Gangetic plain

32   (75°E - 83° E, 23° N - 30° N) where RF at the TOA is positive (+1.27±0.16 W m^{-2}) due to

33   large concentrations of absorbing aerosols. The carbonaceous aerosols produced in-

34   atmospheric heating along the aerosol column extending from the boundary layer to the

35   UTLS (0.01 to 0.3 K d^{-1}) and in the stratosphere globally (0.002 to 0.012 K d^{-1}). The heating

36   of the troposphere increases water vapor concentrations, which are then transported from

37   highly convective region (i.e. the Arabian Sea) to the UTLS (increasing water vapor by 0.02 –

38   0.06 ppmv).

39   Keywords: South Asian Anthropogenic aerosols; warming over the Arabian Sea; transport of

40   aerosols and water vapor to the UTLS in spring.

41

42   **1. Introduction**

43   Understanding the variability of anthropogenic aerosol loading over the North Indian

44   Ocean is of utmost importance since (1) it regulates the Asian hydrological cycle via

45   modulating atmospheric convection, heating rates, and moisture transport (Ramanathan et al.

46   2005; Corrigan et al., 2008; Budhavant et al., 2018, Meehl et al., 2008), and (2) it leads to

47   adverse impacts on marine ecosystems (Mahowald et al., 2018; Collins et al., 2019). Several

48   observations indicate that the aerosol loading over the North Indian Ocean during the spring

49   season is strongly influenced by South Asian aerosols. Aircraft measurements during the

50   Indian Ocean Experiment (INDOEX) (February–March 1999) showed the presence of a thick

51   layer (surface to 3.2 km) of anthropogenic aerosols (BC~14 %, sulfate 34 %, ammonium 11

52   %) over the North Indian Ocean (Dickerson et al., 2002; Mayol-Bracero et al., 2002) with

53   sources over South Asia. Several other in situ observations, e.g. over the Maldives during

54   November 2014 – March 2015, show that air masses arising from the Indo-Gangetic Plain

55   contain very high amounts (97 %) of the elemental carbon in the fine mode. Other

56   anthropogenic species such as organic carbon, non-sea-salt, potassium, and ammonium (70–

57   95%) were also observed in the fine mode (Bhudhvant et al., 2018). Observations from the

58   Geosphere-Biosphere Programme over the Bay of Bengal during spring (March 2016) also

59   show abundant anthropogenic aerosols (sulfate and nitrate) having sources over the Indo-

60   Gangetic plain (Nair et al., 2017).

61   The aerosol loading over South Asia has been increasing at an alarming rate (rate of

62   increase in AOD 0.004 per year during 1988 – 2013) (Babu et al., 2013). For the last two

63   decades, the AOD increase (by 12 %) over south Asia has been attributed to the strong

64   increase in anthropogenic aerosols (sulfate, black carbon, and organic carbon), while natural

65   aerosol remained unchanged (Ramachandran et al., 2020a). The major sources of

66   anthropogenic aerosols are the combustion of domestic fuels, industrial emissions,

67   transportation, and open burning (Paliwal et al., 2016). The growth of the economy of India

68   led to a 41 % increase in BC and 35 % in OC from 2000 to 2010 (Lu et al., 2011). The

69   emissions of sulfur dioxide (SO_2) which leads to the production of sulfate aerosols have

70   doubled during 2006 – 2017 (Fadnavis et al., 2019). Figure 1 a-c shows the annual mean

71   emission of BC, OC, and sulfate aerosols over South Asia in 2016, with high emissions over

72   the Indo-Gangetic Plain (BC 7E-12 – 17E-12 Kg m^{-2} S^{-1}, OC: 25E-12 - 70E-12 Kg m^{-2} S^{-1},

73   sulfate: 2E-12 - 5E-12 Kg m^{-2} S^{-1}). Higher amounts of aerosols over the Indo-Gangetic Plain

74   are associated with densely populated regions and industrial and vehicular emissions

75   (Karambelas et al., 2018, Fadnavis et al., 2019). Past studies also show substantially higher

76   amounts of aerosols over North India compared to rest of the Indian region (Ramachandran et

77   al., 2020b, Fadnavis et al., 2013, 2017a, 2017b). Over the Indo-Gangetic plain, these

78   emissions show a peak in spring (Fig. 1d), with increases for BC of 0 – 3 %, OC 0 – 8.7 %,

79   and sulfate 0 – 0.2 %, compared to annual means. This peak in emissions in spring is to a

80   large extent driven by springtime agricultural crop burning and biomass burning activity

81   (Chavan et al., 2021).

82   While the presence of sulfate aerosols lead to a cooling of the atmosphere below due to

83   their strong scattering properties, carbonaceous aerosols produce atmospheric warming via

84   absorption of solar radiation (Fadnavis et al., 2019, Penner et al., 1998). Previous studies

85   showed that the doubling of carbonaceous aerosols loading over Asia (10° S – 50° N, 65° E–

86   155° E) led to significant atmospheric warming (in-atmospheric RF 5.11W m^{-2}, Fadnavis et al.

87   2017b).

88

89
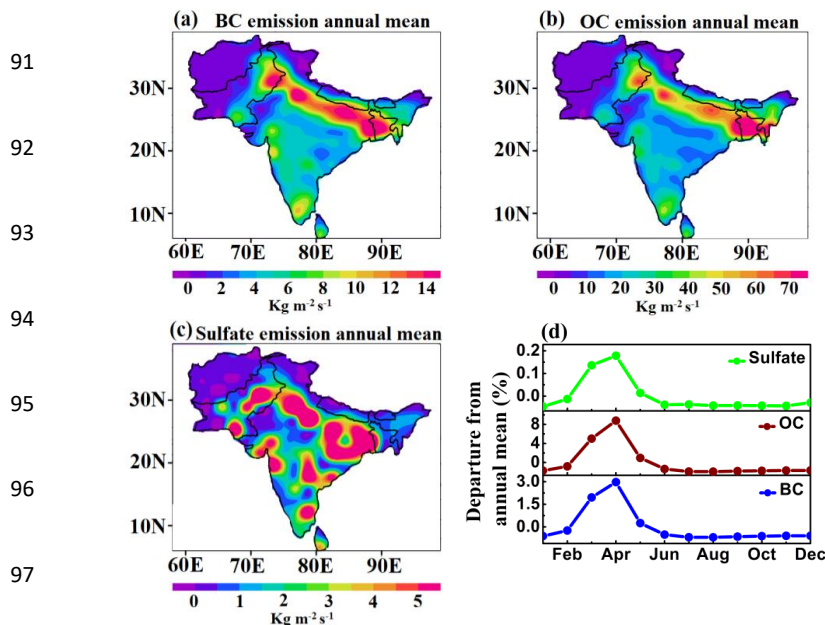
Figure 1: Spatial distribution of year 2016 annual mean total emission (kg m^{-2} S^{-1}) of (a) BC, (b) OC, (c) Sulfate aerosols, (d) time series of monthly departure from annual mean total emissions (%) of BC, OC, and Sulfate aerosols averaged over Indo-Gangetic plain (23° – 30° N, 78 – 90° E).

During spring, the prevailing convective instability over the Bay of Bengal and the Arabian Sea transports aerosol from the boundary layer to the upper troposphere (Romatschke and Houze, 2011). Airborne observations during winter and spring, e.g. the Civil Aircraft for Regular Investigation of the Atmosphere Based on an Instrument Container (CARIBIC) in March 1999 and January 2001 (Papaspiropoulos et al., 2002), and the Indian Ocean Experiment (INDOEX) in February-March 1999 show elevated aerosol amounts near 8 – 12 km over the Indian Ocean and South Asia (De Reus et al., 2001). Recently, using a set of model simulations, Chavan et al., (2021) reported the transport of biomass burning aerosols to the upper troposphere by the convection in spring 2013.

111   Here, we investigate the source of the very large aerosol loading over the Arabian Sea

112   during spring. These aerosols produce atmospheric warming leading to enhanced water vapor

113   that is transported to the UTLS. Once in the lower stratosphere, the water vapour is

114   transported globally, which has implications for tropospheric temperatures and possibly

115   stratospheric ozone. For this purpose, we performed a series of five simulations using the

116   ECHAM6-HAMMOZ model for changes in anthropogenic aerosol over South Asia.

117   **2. Model simulations and satellite data**

118   **2.1 ECHAM6-HAMMOZ experimental set-up**

119   We used the state of art ECHAM6–HAM aerosol–chemistry-climate model. It

120   comprises of the general circulation module ECHAM6, coupled to the aerosol and cloud

121   microphysics module HAM (Stier et al., 2005; Tegen et al., 2019). HAM predicts the

122   nucleation, growth, evolution, and sinks of sulfate, black carbon (BC), particulate organic

123   matter (POM), sea salt (SS), and mineral dust (DU) aerosols. The size distribution of the

124   aerosol population is described by seven log-normal modes with prescribed variance as in

125   the M7 aerosol module (Stier et al., 2005; Zhang et al., 2012). Moreover, HAM explicitly

126   simulates the impact of aerosol species on cloud droplet and ice crystal formation. Aerosol

127   particles can act as cloud condensation nuclei or ice-nucleating particles. Other relevant

128   cloud microphysical processes such as evaporation of cloud droplets, sublimation of ice

129   crystals, ice crystal sedimentation, and detrainment of ice crystals from convective cloud

130   tops are simulated interactively (Neubauer et al., 2014). The anthropogenic and fire

131   emissions of sulfate, black carbon (BC), and organic carbon (OC) are based on the

132   AEROCOM-ACCMIP-II emission inventory. Other details of the model and emissions are

133   reported by Fadnavis et al. (2017a, 2019, 2021a, b).

134   The model simulations are performed at the T63 spectral resolution corresponding to

135   $1.875° \times 1.875°$ in the horizontal dimension, while the vertical resolution is described by 47

136   hybrid $\sigma-p$ levels from the surface up to 0.01 hPa (approx. 80 km). The simulations have

137   been carried out at a time step of 20 min. Monthly varying Atmospheric Model Inter-

138   comparison Project (AMIP) sea surface temperature (SST) and sea ice cover (SIC) (Taylor et

139   al., 2000) were used as lower boundary conditions.

140   We performed five model experiments: (1) a control (CTL) simulation where all aerosol

141   emissions are included and four perturbed experiments where (2) all anthropogenic aerosol

142   emissions (black carbon, organic carbon, and sulfate) are switched off over South Asia (75 –

143   100° E, 8 – 40° N, see Fig. 1) during the study period (2001 – 2016) (referred to as Aerooff),

144   (3) only anthropogenic black carbon emissions (BC) switched off during the study period,

145   (BCoff), (4) only anthropogenic organic carbon (OC) emissions switched off (OCoff) during

146   the study period, and (5) only anthropogenic sulfate aerosol emissions switched off (Suloff)

147   during the study period (see Table 1). All simulations were performed from 1 January 2001 to

148   December 2016 from stabilized initial fields created after a model integration for one year.

149   Dust emission parameterization is the same in all the simulations and is based on Tegen et al.

150   (2002). The analysis is performed for spring (March – May) averaged for the period 2001 –

151   2016. We compare the CTL with Aerooff, BCoff, OCoff, and Suloff simulations to

152   understand the impact of south Asian anthropogenic aerosols over the Indian region and

153   surrounding ocean.

154

155

156

157   Table -1: Details of eECHAM6-HAMMOZ model simulations performed in this study.

Experiment name	Duration	Aerosol species on/off	Boundary conditions
CTL	2001 – 2016	All aerosols species globally, as per AEROCOM-ACCMIP-II emission inventory.	AMIP Sea surface temperature and sea ice concentration.
Aerooff	2001 – 2016	Anthropogenic BC, OC, and sulfate aerosols switch off over South Asia during 2001 – 2016.	AMIP Sea surface temperature and sea ice concentration.
BCoff	2001 – 2016	Anthropogenic BC aerosols switch off over South Asia during 2001 – 2016.	AMIP Sea surface temperature and sea ice concentration.
OCoff	2001 – 2016	Anthropogenic OC aerosols switch off over South Asia during 2001 – 2016.	AMIP Sea surface temperature and sea ice concentration.
Suloff	2001 – 2016	Anthropogenic sulfate aerosols switch off over South Asia during 2001 – 2016.	AMIP Sea surface temperature and sea ice concentration.

158

159   **2.2** AOD satellite observations

160   In this study we use the last fifteen years (2001 – 2016) of aerosol optical depth at 0.55 µm

161   (AOD) obtained from the Moderate Resolution Imaging Spectroradiometer

162   (MODIS) instrument onboard the NASA EOS Terra satellite. The MODIS instrument

163   measure radiance in 36 spectral channels at spatial resolution ranging from 250 m to 1 km

164   with a 2300 km wide swath, allowing for almost daily global coverage. Terra MODIS

165   (MOD08_M3 V6.1) AOD aerosol products are retrieved using the Deep Blue (DB) algorithm

166   (Mhawish et al., 2019). The algorithm calculates the column aerosol loading at 0.55 µm over

167   land and ocean. The AOD data from MODIS Terra can be downloaded from

168   https://ladsweb.modaps.eosdis.nasa.gov/archive/allData/61/MODATML2/

Atmospheric
Chemistry
and Physics
Discussions

Open Access

EGU

169   AOD data from the Multi-angle Imaging Spectro-Radiometer (MISR) for the same period as

170   MODIS (2001 – 2016) is also used for model evaluation. The MISR sensor onboard the Terra

171   satellite has been operational since 1999. It makes measurements at four spectral bands

172   centered at 443 nm, 555 nm, 670 nm, and 865 nm (Diner et al., 2008). In this study we used,

173   level 3 (MIL3MAE_v4) monthly mean aerosol optical depth at 555 nm wavelength at spatial

174   resolution $0.5° \times 0.5°$.   The   MISR   AOD   data   is   available   for   download   at

175   https://misr.jpl.nasa.gov/getData/accessData/.

176

177   **2.3 Model evaluation**

178   We evaluate model performance by comparing simulated AOD (from CTL simulations)

179   with MISR and MODIS data for the spring season. The model simulations show high

180   amounts of AOD over the Indo-Gangetic plain, Myanmar, and East Asia, consistent with

181   MODIS and MISR observations, despite quantitative differences (Fig. 2). Compared to

182   observations, the model underestimates AOD over the Indo-Gangetic plain (model: 0.15 to

183   0.4, MODIS: 0.4 to 0.8, MISR: 0.3 to 0.5) and overestimates AOD over East Asia (model:

184   0.6 to 1.4, MODIS: 0.4 to 1.2, MISR: 0.2 to 0.5). Over the Myanmar region, the model

185   underestimates AOD in comparison to MODIS, but overestimates it in comparison to MISR

186   (model: 0.15 to 0.5, MODIS: 0.3 to 0.8 MISR: 0.15 to 0.3). There are differences among

187   satellite observations and between the model and observations. The differences are due to

188   uncertainties in the model due to model transport processes, emission inventory, and

189   parametrisations (Fadnavis et al. 2014, 2015, 2018, 2019) and there are uncertainties in

190   satellite measurements (Bibi et al., 2015). With model biases present in both the CTL and

191   the perturbed simulations, investigating anomalies removes some of the model bias. In the

192   past Fadnavis et al. (2018, 2019, 2020, 2021a,b) reported model evaluations for AOD,

193   absorbing aerosol index, precipitation, mixing ratio of black carbon aerosol and cloud ice

194 with various measurements that show the fair performance of the ECHAM6-HAMMOZ

195 model.

196
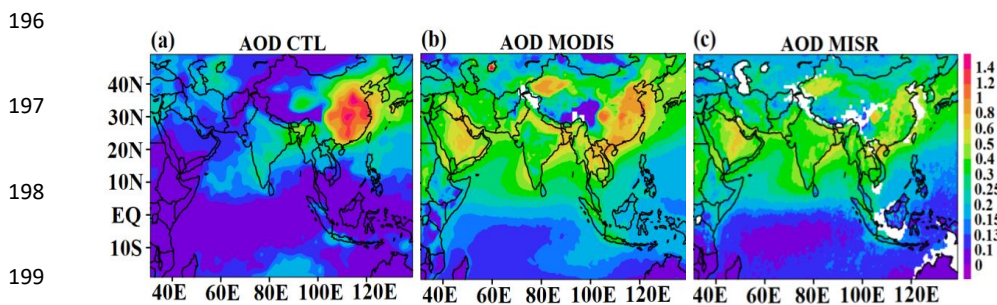
200 Figure 2: Spatial distribution of AOD average for the spring season during 2001 – 2016, from
201 (a) ECHAM6-HAMMOZ CTL simulations, (b) MODIS measurements average for the spring
202 season during 2001 – 2016, (c) MISR measurement average for the spring season during
203 2001 – 2016.

204 **4. Results and discussions**

205 **4.1 Transport of South Asian aerosols to the North Indian Ocean**

206 The spatial distribution of AOD anomalies from the Aerooff simulation shows positive

207 anomalies of AOD extending from South Asia to the Arabian Sea and the North Bay of

208 Bengal (10 - 20° N) (Fig. 3a). The wind vectors indicate that these are transported from the

209 Indo-Gangetic plain to the Arabian Sea and the Bay of Bengal. The transported aerosols

210 enhanced the AOD by 0.18 - 0.8 (30 - 80 %) over the North Bay of Bengal and by 0.02 - 0.12

211 (20 - 60 %) over the Arabian Sea. This is consistent with previous studies where 50 - 60 %

212 enhancements in the AOD over the tropical Indian Ocean due to anthropogenic aerosols have

213 been reported (Satheesh et al. 1999; Jose et al. 2020). Chemical analysis of aerosols observed

214 over the south-eastern coastal Arabian Sea also shows the dominance of anthropogenic

215 aerosols having sources over the Indian region (73 %) (Aswini et al., 2020). Analysis of

216 MODIS satellite observations (2003 – 2017) likewise shows that anthropogenic sources

217 contributed ~60 – 70% to the aerosol loading over the east coast and west coast of India (Jose

218   et al. 2020). Measurements over the Equatorial Indian Ocean further show a substantial

219   increase in AOD (~80 %) due to anthropogenic aerosols (Gogoi et al., 2019).

220
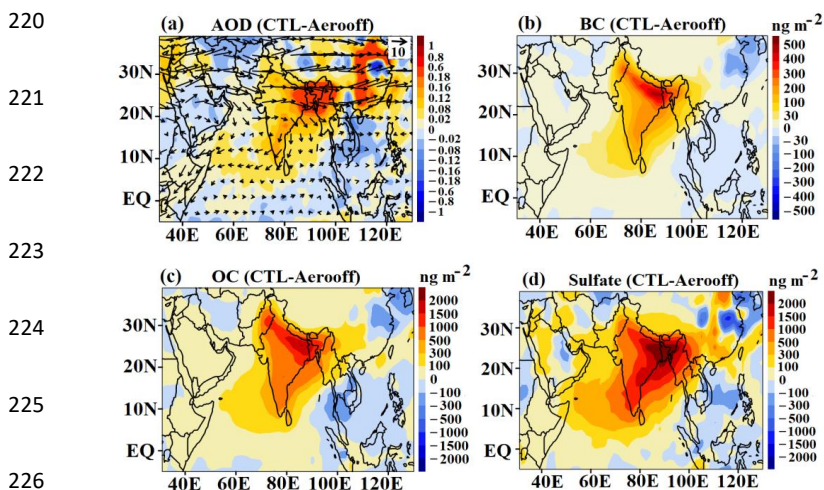
227   Figure 3: Spatial distribution of (a) AOD anomalies averaged for spring during 2001 –
228   2016 (CTL - Aerooff), and anomalies of tropospheric column of (b) BC, (c) OC, and (d)
229   sulfate aerosols (ng m^{-2}) (CTL-Aerooff). The vectors in Fig.1a indicate winds (m s^{-1}) at
230   850 hPa.

231 The distribution of anomalies in the tropospheric column of BC, OC, and sulfate aerosols also

232 indicates that these aerosols are transported from South Asia to the Bay of Bengal and the

233 Arabian Sea (Fig. 3b-d). Enhancement of sulfate and OC aerosol (100 – 2000 ng m^{-2}) is

234 higher than BC (100 – 500 ng m^{-2}) over the South Asian region (Fig. 3b-d). The total

235 carbonaceous aerosol (BC and OC together) dominates over the sulfate aerosols. These

236 anthropogenic aerosols over the tropical Indian Ocean affect the radiation budget and cloud

237 cover over the Indian Ocean (Satheesh et al. 1999; McFarquhar and Wang 2006).

238

239

Atmospheric
Chemistry
and Physics
Discussions

3.2. Radiative forcing

240

241 The anthropogenic aerosols over the tropical Indian Ocean affect the radiation budget and

242 cloud cover (McFarquhar and Wang 2006). Here, we discuss the impact of south Asian

243 anthropogenic aerosols on radiative forcing (RF). Figures 4a-c show anomalies in net

244 radiative forcing (RF) at the TOA, surface, and in-atmosphere (TOA - surface) for Aerooff

245 simulations (CTL - Aerooff). The anthropogenic aerosols have produced a cooling at the

246 TOA (except over the Indo-Gangetic plain) and surface (see Fig. 4a-b). The simulated RF

247 values over the Arabian Sea (55 – 70° E, 8 – 20° N), Bay of Bengal (88 – 92° E, 12 – 20° N),

248 and Indo-Gangetic Plain (75 – 83° E, 26 – 30° N) are tabulated in Table-S1. The RF

249 estimates show that aerosols have produced significant cooling at the TOA and surface over

250 the Arabian Sea (TOA: -0.72 ± 0.14 W m^{-2}, surface:-3.0 ± 0.28 W m^{-2}), Bay of Bengal (TOA:-

251 1.24 ± 0.15 Wm^{-2}, surface: -5.14 ± 0.44 W m^{-2}), and in-atmospheric warming over the above

252 regions (Arabian Sea $+2.27\pm0.19$ W m^{-2}; Bay of Bengal: $+3.89\pm0.30$ W m^{-2}) (Fig. 4 c). The

253 Indo Gangetic Plain shows positive anomalies of RF at the TOA ($+1.27\pm0.16$ Wm^{-2}),

254 negative at the surface (-11.16 ± 0.50 Wm^{-2}), and atmospheric warming of $+12.44\pm0.42$ W m^{-2}

255 ^{2}. In agreement with our results, several previous studies have reported negative RF at the

256 surface and TOA, and atmospheric warming over the north Indian Ocean caused by enhanced

257 anthropogenic aerosol. For example, Pathak et al. (2020) reported negative aerosol RF at the

258 TOA (-2 to -4 W m^{-2}) over the Bay of Bengal and the Arabian Sea during spring 2009 - 2013.

259 Reddy et al., (2004) estimated positive in-atmosphere RF over the North Indian Ocean ($+25$

260 W m^{-2}). The aerosol radiative forcing estimated from satellite measurements (January to

261 March 1999) over the north Indian ocean is also negative at TOA (-4 and -14 W m^{-2}) and

262 surface (-12 to -42 W m^{-2}) (Satheesh and Ramanathan 2000; Rajeev and Ramanathan et al,

263 2001). The clear sky aerosol direct radiative forcing estimated from measurements during the

264 INDOEX experiment (January to March in 1999) over the north Indian Ocean also show

265 similar results (TOA: -7 W m^{-2}, surface: -23 W m^{-2}, and in-atmosphere: +16 W m^{-2})

266 (Ramanathan et al. 2001). These studies attribute positive in-atmospheric radiative forcing to

267 absorbing aerosols (especially black carbon) that lead to heating of the atmosphere (Rajeev

268 and Ramanathan 2001; Satheesh et al 2002).

269   Analysis of the perturbed model experiments indicates that anthropogenic BC

270 aerosols (Fig. 4d-f) have produced a warming at the TOA (Arabian Sea: 1.24±0.13 W m^{-2},

271 Bay of Bengal: 1.54±0.26 W m^{-2}, Indo-Gangetic Plain: 4.33±0.17 W m^{-2}) and cooling at the

272 surface (Arabian Sea: -2.56±0.25 W m^{-2}, Bay of Bengal: -3.70±0.49 W m^{-2}, Indo-Gangetic

273 Plain:-9.27±0.37 W m^{-2}). OC (Fig. 4g-i) and sulfate (Fig. 4j-l) aerosols have produced

274 significant cooling at the TOA (OC: -0.21±0.13 to -0.44±0.15 W m^{-2}; Sulfate: -1.55±0.16 to -

275 2.14±0.17 W m^{-2}) and surface (OC: -0.49±0.31 to -2.56±0.45 W m^{-2}, Sulfate: -1.19±0.24 to -

276 2.67±0.36 W m^{-2}) over the above regions (listed in Table-S1). Figures 4d, 4g, and Fig. 4j

277 further confirm our finding that the positive anomalies of radiative forcing in the Indo-

278 Gangetic plain are due to BC aerosols because of its absorbing property. All the aerosols

279 produce in-atmospheric warming over the Indian region and the north Indian Ocean. The

280 atmospheric warming over the Arabian Sea and Bay of Bengal is due to BC and OC aerosols

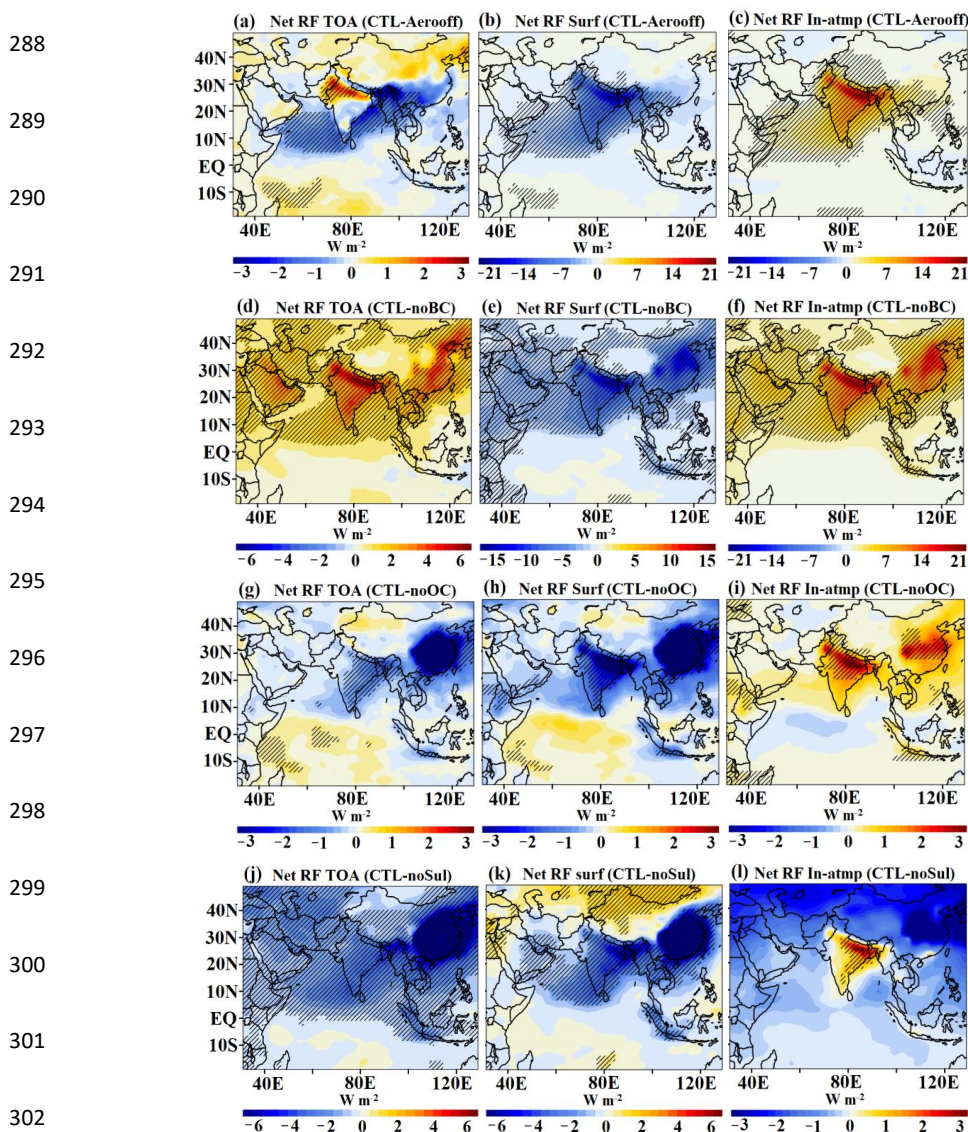281 with larger contributions by the BC aerosols.

282

283

284

285

286

287

Atmospheric
Chemistry
and Physics

Open Access

EGU

Discussions

Figure 4: Spatial distribution of net aerosol radiative forcing (CTL - Aerooff) (W m^{-2})
averaged for spring during 2001 – 2016 (a) TOA, (b) same as (a) but for surface, (c) same
as (a) but for in-atmosphere (TOA - surface), (d) spatial distribution of radiative forcing at
the TOA (CTL – BCoff) averaged for spring during 2001 – 2016, (e) same as (d) but for
surface, (f) same as (d) but for in-atmosphere (TOA - surface), (g) spatial distribution of
radiative forcing at the TOA (CTL - OCoff) averaged for spring during 2001 – 2016, (h)
same as (g) but for surface, (i) same as (h) but for in-atmosphere (TOA - surface), (j)
spatial distribution of radiative forcing at the TOA (CTL - Suloff) averaged for spring
during 2001 – 2016, (k) same as (j) but for surface, (l) same as (k) but for in-atmosphere
(TOA - surface). The hatched lines in figure a-l indicate 99% confidence level for the
mean differences.

314   3.3. Transport of Asian anthropogenic aerosols into the UTLS

315   Further, we investigate the vertical distribution of aerosols that are transported to the north

316   Indian Ocean. Meridional sections over the Arabian Sea (60 – 75° E) and Bay-of-Bengal (75

317   – 95 °E) for BC, OC, and sulfate aerosol anomalies indicate that these aerosols are

318   transported from the boundary layer of both regions and north India into the UTLS (Figure 5

319   and Fig. S1). The spring convection occurring over the Arabian Sea and Bay-of-Bengal

320   which is shown by the combined distribution of CDNC and ICNC (Fig. S2a) plays an

321   important role in the vertical transport. The prevailing spring convection is further

322   invigorated over the Arabian Sea by the transported aerosols there which is not the case for

323   the Bay of Bengal region (Fig. S2b). The aerosol loading over the North-Indian region forms

324   clouds and elicit convection there (Fig. S2c-d). The distribution of wind resolved circulation

325   shows a strong ascent over the Arabian Sea, and the Bay-of-Bengal regions, while the steep

326   orography of the Himalayas over North India also plays an important role in the vertical

327   transport to the upper troposphere (Fig. 5 and Fig. S1). Figure 5 also shows that aerosols

328   induce a secondary circulation, ascending winds over 10 – 30° N and descent over 30 – 40°

329   S. BC, OC, and sulfate aerosols are transported to the UTLS, moving southward and

330   downward ~30 – 40° S (Fig. 5a-f, and Fig. S1) due to this secondary circulation. The aerosol

331   enhancement in the lower troposphere (1000 – 500 hPa) over 30 – 40° S is therefore due to

332   the combined impact of horizontal transport and downward transport from the UTLS due to

333   this secondary circulation. Further, in the UTLS these aerosols are transported globally.

334   There is enhancement in the Arctic (BC: 0.6 to 1.5 ng m^{-3}, OC: 0.4 to 7 ng m^{-3}, Sulfate: 0.1 to

335   20 ng m^{-3}) and Antarctic (BC: 0.6 to 3 ng m^{-3}, OC: 1 to 5 ng m^{-3}, Sulfate: 6 to 40 ng m^{-3}) in

336   the lower stratosphere (180 – 90 hPa) (see Figure 5). Our analysis shows that transport to the

337   Arctic and Antarctic occurs every year in the UTLS which causes heating in the lower

338   stratosphere (see Section 3.4).

339
340
341
342
343
344
345
346
347
348
349
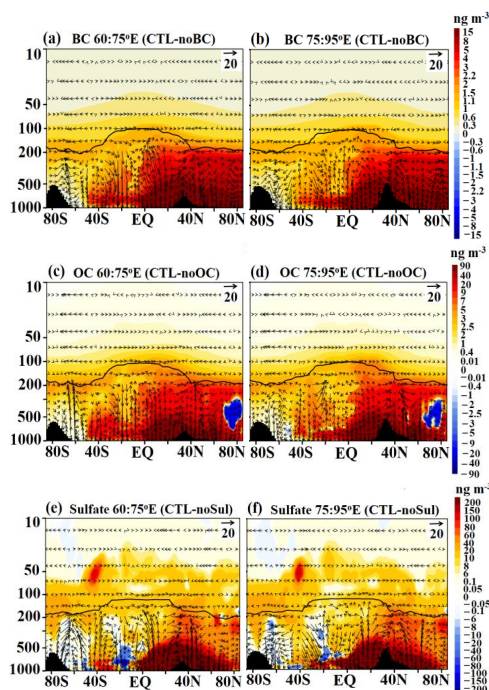
350 Figure 5: Meridional cross-section over Arabian Sea (averaged 60 – 75° E) and Bay-of-
351 Bengal (75 – 95° E) and for the spring season during 2001 – 2016 of anomalies (ng m^{-3}) of
352 (a–b) BC aerosols (CTL-BCoff), (c–d) OC aerosols (CTL-OCoff), (e–f) sulfate aerosols
353 (CTL-Suloff). Vectors in Figs. a-f indicate anomalies of winds (m s^{-1}) (the vertical velocity
354 field has been scaled by 300 and the units are m s^{-1}).

355

356 **3.4. Impacts on the heating rate and water vapor**

357   Carbonaceous aerosols absorb solar radiation, leading to atmospheric heating, while

358 predominately scattering aerosols such as sulfate reflect and scatter back solar radiation,

359 therefore cooling the atmosphere below (Fadnavis et al., 2019). The vertical distribution of

360 heating rate anomalies induced by all the anthropogenic Asian aerosols (CTL - Aerooff) over

361 the North Indian Ocean (Arabian Sea and North Bay of Bengal, 50 – 100° E) indicates a

362 significant increase in heating rates in the region of elevated anthropogenic aerosols in the

363 troposphere (0.05 K d^{-1}) and stratosphere (0.002 K d^{-1}) (Fig. 6a-d, Fig. 5, and Fig. S1).

364 Heating rate anomalies estimated over the North Indian Ocean from BC (CTL - BCoff), OC

365   (CTL - OCoff), and Sulfate (CTL - Suloff) show that BC and OC aerosols produce heating in

366   the troposphere (10 – 40º N) (BC: 0.001 to 0.05 K d^{-1}, OC: 0.0002 to 0.02 K d^{-1}) and

367   stratosphere (100 – 50 hPa, 90ºS – 90ºN) (BC: 0.001 to 0.008 K d^{-1}, OC: 0.0002 to 0.002 K

368   d^{-1}), while sulfate aerosols produce atmospheric cooling in the troposphere -0.001 to -0.05

369   (500 – tropopause) and stratosphere -0.001 to -0.008 K d^{-1} (tropopause – 50 hPa) (Fig. 6a-d).

370   There is anomalous heating in the tropical stratosphere (20° S – 20° N) (0.001 to 0.002 K d^{-1})

371   seen in CTL-Aerooff simulations (Fig. 6a), mainly due to carbonaceous aerosols (Fig. 6b-c).

372   The zonal mean distribution of heating rates (Fig 6 e-h) shows that the South Asian

373   carbonaceous aerosols lead to 0.002 – 0.01 K d^{-1} heating in the lower stratosphere globally

374   (100 – 50 hPa) (Fig. 6f-g), larger than the cooling induced by sulfate aerosols (Fig. 6h).

375
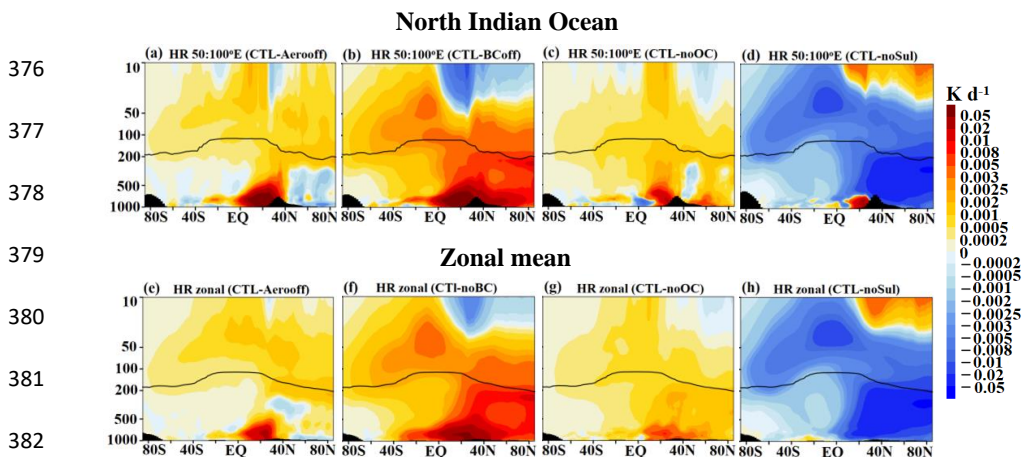
Figure 6: Meridional cross-section over the North Indian Ocean (averaged over the Arabian Sea and Bay of Bengal region, 50 – 100° E) of anomalies of heating rates (K d^{-1}) averaged for the spring season during 2001 – 2016 (a) from CTL - Aerooff simulation, (b) same (a) but from CTL - BCoff simulation (c) same (a) but from CTL -OCoff simulation, (d) same (a) but from CTL - Suloff simulation. (e) Zonal mean (0 –360°) anomalies in heating rate for CTL - Aerooff simulation, (f) same as (e) but from CTL - BCoff simulation, (g) same as (e) but from CTL - OCoff simulation, (h) same as (e) but from CTL - Suloff simulation.

391   In general, these aerosols increase heating in the troposphere over the South Asian region

392   (Fig. 6a) and northern Arabian Sea and Bay of Bengal (10 – 30° N). This enhanced heating

393   invigorates the convection process, which results in an increase in cloud cover (Fig. S2c) and

394   deepening of the OLR (Fig. S2d). The invigorated convection provides positive feedback on

395   the vertical ascent into the free troposphere that extends to above the tropopause into the

396   lower stratosphere over the Arabian Sea and Bay-of-Bengal-North-India region (Fig. S3a-b)

397   (Fadnavis et al., 2013; Randel et al., 2010).

398   The vertical distribution of water vapor over the Indian Ocean (CTL - Aerooff) shows that

399   water vapor (0 – 0.3 ppmv) is transported to the UTLS from the Arabian Sea (55 – 70° E, 0 –

400   30° N) (Fig. 7a) along the path of elevated aerosols (Fig. 5). Interestingly, there is an

401   enhancement in water vapor over the southern Indian Ocean (20 – 30° S, 55 – 70° E) along

402   the path of the descending branch of aerosols (BC, OC, and sulfate). This is due to the

403   significant heating caused by carbonaceous aerosols (Fig. 6b-c) which leads to enhancement

404   of tropospheric water vapor (Fig. 7a) over the Arabian Sea. The zonal mean (averaged for 0 –

405   360°) anomalies of water vapor (Fig. 7b) show an enhancement by 0.03-0.08 ppmv (0 – 4 %)

406   in the global stratosphere (Fig. 7b). There is an enhancement in the lower stratosphere in the

407   Antarctic (60 – 90º S) by 0.01 to 0.03 ppmv and in the Arctic (80 – 90º N) by 0.01 - 0.1 ppmv

408   caused by anthropogenic aerosols (CTL-Aerooff).

409   The impact of BC (CTL - BCoff), OC (CTL - OCoff), and Sulfate (CTL - Suloff) on water

410   vapor distribution (Figs. 7 c-f) shows that BC aerosols play a major role in water vapor

411   enhancement in the stratosphere (Fig. 7 c), (100 – 10 hPa). Water vapor enhancement by BC

412   aerosols over the Arabian Sea region is ~0.03 – 0.3 ppmv (Fig. 7c) and 0.01 – 0.2 ppmv in

413   the global stratosphere (Fig. 7d). There is significant enhancement of water vapor due to BC

414   aerosols in the Arctic (0.01 – 0.2 ppmv) and Antarctic (0.01 – 0.1 ppmv) (Fig. 7d). The water

415   vapor enhancement by OC aerosols is negligible in the tropical stratosphere and there is no

416 contribution of sulfate aerosols (Fig. 7 e-f). The sulfate aerosols cause negligible heating by

417 abortion of infra-red radiations over the Arabian Sea that leads to water vapor enhancement

418 from the boundary layer to the mid-troposphere (500 hPa), near the tropopause, and in the

419 path of descending branch of secondary circulation over the South Indian Ocean (~20° S)

420 (Fig. 7f).
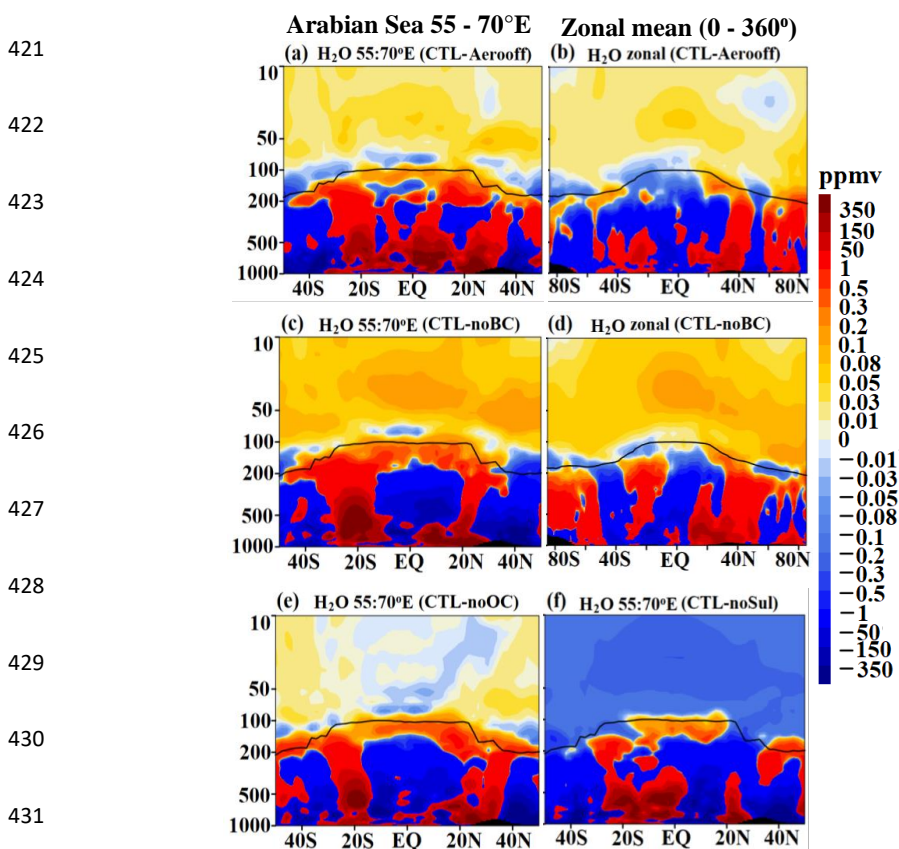
432 Figure 7: (a) Meridional cross-section over Arabian Sea region (averaged 55 – 70° E) of
433 anomalies of water vapour (ppmv) (CTL - Aerooff) the for spring season during 2001 – 2016,
434 (b) same as (a) but zonal mean (average for longitudes 0 – 360°), (c) same as (a) but from
435 CTL - BCoff simulations, (d) same as (c) but zonal mean (average for longitudes 0 –360°),
436 (e) same as (a) but from CTL - OCoff simulations, (f) same as (a) but from CTL - Suloff
437 simulations.

438 Although the focus of the manuscript is on transport of aerosols during the spring season, it

439 should be noted that the anthropogenic South Asian aerosols are also transported to the UTLS

440   during the monsoon season (Fadnavis et al., 2013, 2017, 2019). Annual distribution

441   anomalies of aerosols (average of BC, OC and sulfate) show transport of aerosols into the

442   UTLS during spring and monsoon season (April to September) from the Arabian Sea, Bay-

443   of-Bengal-North-India region (Fig. 8a). These aerosols enhance tropospheric heating thereby

444   transporting elevated water vapour into the lower stratosphere (Fig. 8b). Injection of aerosols

445   into the lower stratosphere occurs every year however there is interannual variability. We

446   show the vertical distribution of aerosols for two normal years when there was no large scale

447   ocean-atmosphere coupling phenomenon like El Niño southern oscillation or Indian Ocean

448   Dipole (2008 and 2016) in Fig. S4a-b. It also shows transport of aerosols into the lower

449   stratosphere during spring and monsoon seasons (March-September). The aerosol induced

450   enhanced water vapour also shows enhancement in the lower stratosphere during the same

451   time (Figs. S4c-d). In the lower stratosphere, these aerosols persist for a few months (Fig. 8a)

452   thus their effect will be seen for an extended time.

453
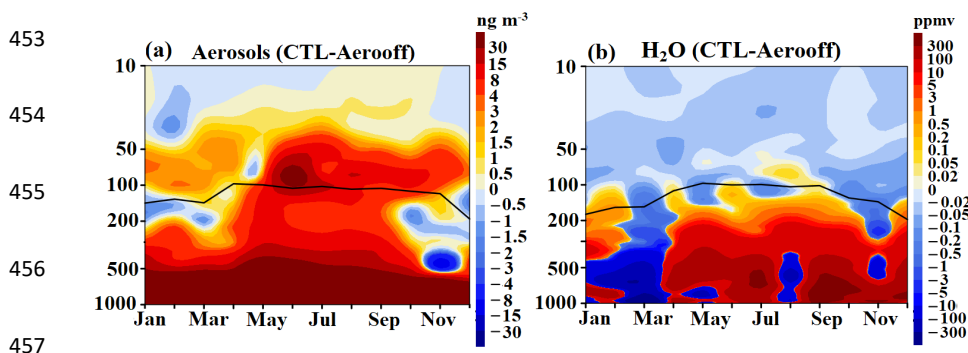
458   Figure 8: (a) Annual distribution of anomalies of aerosols (CTL - Aerooff) (averaged of BC,

459   OC and sulfate aerosols) (ng m^{-3}) averaged for Arabian Sea, Bay-of-Bengal-North-India

460   region (55 – 110° E, 10 – 30° N), (b) same as (a) but for water vapour (ppmv).

461   Further, we analyze the correlation between heating rates and carbonaceous aerosol amounts

462   in the UTLS (180 – 70 hPa) in the Arctic and Antarctic during 2001 – 2016 (spring mean)

463   (Fig. 9) from Aerooff, BCoff, and OCoff in comparison with CTL simulations. The

464   carbonaceous aerosols show a positive correlation (correlation coefficient r: 0.57 to 0.94)

465   with the UTLS heating rates indicating that transported carbonaceous aerosols enhance UTLS

466   heating in the Arctic and Antarctic. It should be noted that transport of aerosols to the Arctic

467   and Antarctic also occurs during the monsoon season (Fadnavis et al., 2017a, 2017b, 2019)

468   which may affect the dynamics and aerosol amounts in the spring of the next year in the

469   UTLS.
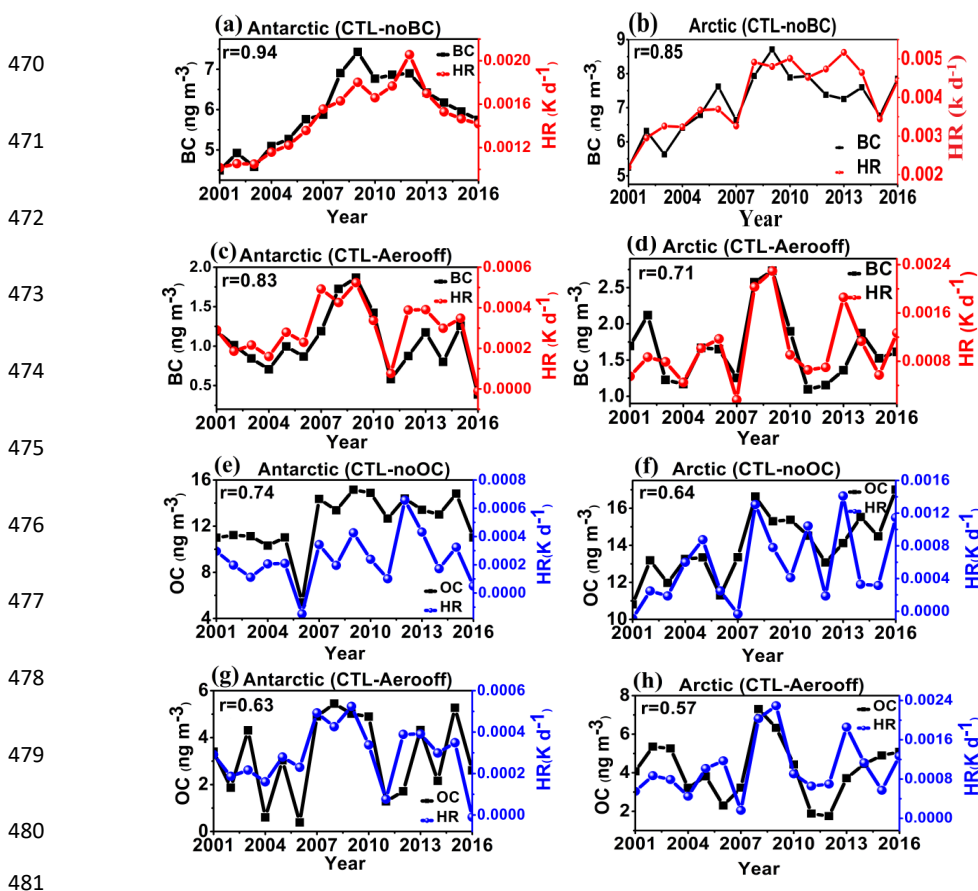
Figure 9: (a) Time series of BC aerosols and heating rates averaged for spring and UTLS (180 – 70 hPa) at the Antarctic (60 – 90 °S, 0 – 360 °)(from CTL - BCoff, (b) same as (a) but in the Arctic (65 – 85° N, 0 – 360°), (c) same as (a) but from CTL - Aerooff, (d) same as (b) but from CTL - Aerooff, (e) same as (a) but for OC (CTL - OCoff), (f) same as (b) but for OC (CTL - OCoff), (g) same as (c) but for OC, (h) same as (d) but for OC. The correlation coefficient (r) between anomalies of BC/OC aerosols and heating rates is indicated in panels a-h.

489   Importantly, South Asian aerosols enhance water vapor in the lower stratosphere, globally.

490   Water vapor being a greenhouse gas further enhances the heating of the troposphere leading

491   to a positive feedback. The increase in water vapor in the stratosphere also warms the Earth's

492   surface (Shindell, 2001; Solomon et al., 2010). Solomon et al. (2010) estimated that an

493   increase in the stratospheric water vapor by 1 ppmv accounts for 0.24 W m^{-2} radiative

494   forcing. The SABER and MLS observations showed an increase in stratospheric water vapor

495   by 0.45 ppmv globally during 2003 – 2017 (Yue et al., 2019). Thus the radiative forcing due

496   to water vapor increase (0.02 – 0.14 ppmv) in response to South Asian anthropogenic

497   aerosols is not negligible for surface warming globally. Further, increasing stratospheric

498   water vapour could also lead to ozone depletion (e.g., Shindell, 2001, Robrecht et al., 2019).

499   **4. Conclusions**

500   A series of ECHAM6-HAMMOZ chemistry-climate simulations for South Asian

501   anthropogenic aerosols were used to understand the transport pathways of Asian aerosols and

502   their associated impacts. The analysis is performed for the spring season, when emissions of

503   anthropogenic aerosols (BC, OC, and sulfate) over south Asia peak. The model simulations

504   show that large amounts of South Asian aerosols are transported during spring to the Arabian

505   Sea (increases in AOD by: 0.02 – 0.12 from CTL - Aero0ff) and Bay of Bengal (increases in

506   AOD by: 0.16 to 0.8 from CTL - Aerooff). The anthropogenic aerosols are further lifted up

507   into the UTLS from the Arabian Sea and Bay-of-Bengal-North-India. In the UTLS, they are

508   also transported to the southern hemisphere (30 – 40 °S) and downward in the troposphere by

509   the secondary circulation induced by the aerosol changes. In the UTLS, these aerosols (BC,

510   OC, and Sulfate) are transported globally.

511   The anthropogenic aerosol produces significant radiative impacts over the Indo-Gangetic

512   Plain (RF anomalies estimated from CTL-Aerooff simulations, TOA: +1.27±0.16 W m^{-2},

513   Surface: -11.16±0.50 W m^{-2}, In-atmosphere: +12.44±0.42 W m^{-2}) and the Arabian Sea (RF at

514   the TOA: -0.72±0.14 W m^{-2}, surface: -3.00±0.28 W m^{-2}, In-atmosphere: +2.27±0.19 W m^{-2}).

515   Interestingly, RF at the TOA over the Indo-Gangetic Plain is positive +4.33±0.17 W m^{-2} due

516   to the emission of BC aerosols. The anthropogenic aerosols enhance heating in the

517   troposphere (estimated from CTL-Aerooff) by 0.002 to 0.05 K d^{-1} and UTLS by 0.001 to

518   0.002 K d^{-1} leading to more cloud formation (cloud cover anomalies enhanced by 2 to 12 %)

519   and intensification of convection (OLR anomalies -0.5 to -10 W m^{-2}). This invigorated

520   convection provides a positive feedback on the vertical updraft of aerosols into the free

521   troposphere and above the tropopause into the lower stratosphere (Fadnavis et al., 2013;

522   Randel et al., 2010). The tropospheric heating/cooling caused by the anthropogenic aerosols

523   over South Asia and the North Indian Ocean during spring has implications on the Indian

524   summer monsoon rainfall a few months later (Fadnavis et al., 2017a; Fadnavis and

525   Chattopadhyay, 2017).

526

527   The heating of the troposphere by the carbonaceous aerosol increases evaporation and

528   thereby tropospheric water vapor amounts over the North Indian Ocean and adjoining

529   regions. The elevated water vapor is transported from highly convective regions (i.e. Arabian

530   Sea) to the UTLS, from where it is then transported globally. BC aerosols play a major role in

531   water vapor enhancement in the lower stratosphere, globally (increased water vapor by 0.01

532   to 0.1 ppmv). Water vapor being a greenhouse gas further enhances the heating of the

533   troposphere leading to a positive feedback. The increase in water vapor in the stratosphere

534   also warms the Earth's surface (Shindell, 2001; Solomon et al., 2010).

537   **Data availability:** The data used in this study are generated from ECHAM6-HAMMOZ

538   model simulations at the High-performance computing system in the Indian Institute of

539   Tropical Meteorology, Pune, India. The AOD data from MODIS Terra used here can be

540   downloaded from https://ladsweb.modaps.eosdis.nasa.gov/archive/allData/61/MODATML2/,

541   and MISR from https://misr.jpl.nasa.gov/getData/accessData/.

542

543

544   **Author contributions**: S. F. initiated the idea. A. J., S. S., A. A., performed model analysis.

545   R. M., and A. R. contributed to analysis and study design. All authors contributed to the

546   writing and discussions of the manuscript.

547

548   **Competing Interests**: Some authors are members of the editorial board of Atmospheric

549   Chemistry and Physics. The peer-review process was guided by an independent editor, and

550   the authors have also no other competing interests to declare.

551

References:

Aswini, A. R., Hegde, P., Aryasree, S., Girach, I. A. and Nair, P. R.: Continental outflow of anthropogenic aerosols over Arabian Sea and Indian Ocean during wintertime: ICARB-2018 campaign, Sci. Total Environ., 712, 135214, doi:10.1016/j.scitotenv.2019.135214, 2020.

Babu, S. S., Manoj, M. R., Moorthy, K. K., Gogoi, M. M., Nair, V. S., Kompalli, S. K., Satheesh, S. K., Niranjan, K., Ramagopal, K., Bhuyan, P. K. and Singh, D.: Trends in aerosol optical depth over Indian region: Potential causes and impact indicators, J. Geophys. Res. Atmos., 118, 11,794-11,806, doi:10.1002/2013JD020507, 2013.

Bibi H., Alam K., Chishtie F., Bibi S., Shahid I, Blaschke T., Intercomparison of MODIS, MISR, OMI, and CALIPSO aerosol optical depth retrievals for four locations on the Indo-Gangetic plains and validation against AERONET data, Atmospheric Environment, 111, 113-126, https://doi.org/10.1016/j.atmosenv.2015.04.013, 2015.

Budhavant, K., Bikkina, S., Andersson, A., Asmi, E., Backman, J., Kesti, J., Zahid, H., Satheesh, S. K. and Gustafsson, Ö.: Anthropogenic fine aerosols dominate the wintertime regime over the northern Indian Ocean, Tellus, Ser. B Chem. Phys. Meteorol., 70, 1–15, doi:10.1080/16000889.2018.1464871, 2018.

Chavan, P., Fadnavis, S., Chakroborty, T., Sioris, C. E. and Müller, R.: The outflow of Asian biomass burning carbonaceous aerosol into the UTLS in spring: Radiative effects seen in a global model, 21, 14371–14384, https://doi.org/10.5194/acp-2021-494, 2021.

Corrigan, C. E., Roberts, G. C., Ramana, M. V., Kim, D. and Ramanathan, V.: Capturing vertical profiles of aerosols and black carbon over the Indian Ocean using autonomous unmanned aerial vehicles, Atmos. Chem. Phys., 8, 737–747, doi:10.5194/acp-8-737-2008, 2008.

Atmospheric
Chemistry
and Physics
Discussions

576 Collins, M., Sutherland, M., Bouwer, L., Cheong, S.-M., Frölicher, T. L., Jacot Des Combes,

577   H., Roxy, M. K., Losada, I., McInnes, K. L., Ratter, B., Rivera-Arriaga, E., Susanto, R.

578   D., Swingedouw, D., Tibig, L., Bakker, P., Eakin, C. M., Emanuel, K., Grose, M.,

579   Hemer, M., Jackson, L., Kääb, A., Kajtar, J. B., Knutson, T., Laufkötter, C., Noy, I.,

580   Payne, M., Ranasinghe, R., Sgubin, G. and Timmermans, M.-L.: Extremes, Abrupt

581   Changes and Managing Risks, IPCC Spec. Rep. Ocean Cryosph. a Chang. Clim., 589–

582   655, 2019.

583 De Reus, M., Krejci, R., Williams, J., Fischer, H., Scheele, R. and Ström, J.: Vertical and

584   horizontal distributions of the aerosol number concentration and size distribution over

585   the northern Indian Ocean, J. Geophys. Res. Atmos., 106, 28629–28641,

586   doi:10.1029/2001JD900017, 2001.

587 Dickerson, R. R., Andreae, M. O., Campos, T., Mayol-Bracero, O. L., Neusuess, C. and

588   Streets, D. G.: Analysis of black carbon and carbon monoxide observed over the Indian

589   Ocean: Implications for emissions and photochemistry, J. Geophys. Res. Atmos., 107,

590   doi:10.1029/2001JD000501, 2002.

591 Diner, D. J., Abdou, W. A., Ackerman, T. P., Crean, K., Gordon, H. R., Kahn, R. A.,

592   Martonchik, J. V., Mcmuldroch, S., Paradise, S. R., Pinty, B., Verstraete, M. M.,

593   Wang, M., West, R. A. Level 2 aerosol retrieval algorithm theoretical basis, Jet

594   Propuls. Lab. Intern. Doc. JPL D-11400, Rev C, 2008.

595 Fadnavis, S., Kalita, G., Rowlinson, M., Rap, A., Li, J.-L. F., Gasparini, B., Laakso, A. and

596   Müller, R.: The impact of increases in South Asian anthropogenic emissions of SO_2 on

597   sulfate loading in the upper troposphere and lower stratosphere during the monsoon

598   season and the associated radiative changes, Atmos. Chem. Phys., 19, 9989–10008,

599   https://doi.org/10.5194/acp-19-9989-2019, 2019.

600 Fadnavis, S., Roy, C., Chattopadhyay, R., Sioris, C. E., Rap, A., Müller, R., Kumar, K. R.

601 and Krishnan, R.: Transport of Asian trace gases via eddy shedding from the Asian

602 summer monsoon anticyclone and associated impacts on ozone heating rates, Atmos.

603 Chem. Phys., 18, 11493–11506, doi:10.5194/ acp-18-11493-2018, 2018.

604 Fadnavis, S., Roy, C., Sabin, T. P., Ayantika, D. C. and Ashok, K.: Potential modulations of

605 pre-monsoon aerosols during El Niño: impact on Indian summer monsoon, Clim. Dyn.,

606 49, 2279–2290, doi:10.1007/s00382-016-3451-6, 2017a.

607 Fadnavis, S., Kalita, G., Ravi Kumar, K., Gasparini, B. and Li, J. L. F.: Potential impact of

608 carbonaceous aerosol on the upper troposphere and lower stratosphere (UTLS) and

609 precipitation during Asian summer monsoon in a global model simulation, Atmos.

610 Chem. Phys., 17, 11637–11654, doi:10.5194/acp-17-11637-2017, 2017b.

611 Fadnavis, S. and Chattopadhyay, R.: Linkages of subtropical stratospheric intraseasonal

612 intrusions with Indian summer monsoon deficit rainfall, J. Clim., 30, 5083–5095,

613 doi:10.1175/JCLI-D-16-0463.1, 2017.

614 Fadnavis S., Semeniuk K., Schultz M.G., Kiefer M., Mahajan A., Pozzoli L., Sonbawane S.,

615 Transport pathways of peroxyacetyl nitrate in the upper troposphere and lower

616 stratosphere from different monsoon systems during the summer monsoon season,

617 Atmospheric Chemistry and Physics, 15, 11477-11499, DOI:10.5194/acp-15-11477-

618 2015, 2015.

619 Fadnavis S., Schultz M.G., Semeniuk K., Mahajan A.S., Pozzoli L., Sonbawane S., Ghude

620 S.D., Kiefer M., Eckert E., Trends in Peroxyacetyl Nitrate (PAN) in the upper

621 troposphere and lower stratosphere over Southern Asia during the summer monsoon

622 season: regional impacts., Atmospheric Chemistry and Physics, 14, 12725-12743,

623 DOI:10.5194/acp-14-12725-2014, 2014.

624 Fadnavis, S., Semeniuk, K., Pozzoli, L., Schultz, M. G., Ghude, S. D., Das, S. and Kakatkar,

625   R.: Transport of aerosols into the UTLS and their impact on the asian monsoon region

626   as seen in a global model simulation, Atmos. Chem. Phys., 13, 8771–8786,

627   doi:10.5194/acp-13-8771-2013, 2013.

628   Fadnavis, S., Sioris, C. E., Wagh, N., Chattopadhyay, R., Tao, M., Chavan, P. and

629   Chakroborty, T.: A rising trend of double tropopauses over South Asia in a warming

630   environment: Implications for moistening of the lower stratosphere, Int. J. Climatol.,

631   41, E200–E215, doi:10.1002/joc.6677, 2020.

632   Fadnavis, S., Sabin, T. P., Rap, A., Müller, R., Kubin, A. and Heinold, B.: The impact of

633   COVID-19 lockdown measures on the Indian summer monsoon, Environ. Res. Lett.,

634   16, 074054, doi:10.1088/1748-9326/ac109c, 2021a.

635   Fadnavis S., Müller R , Chakraborty T. , Sabin T. P., Laakso A. , Rap A. , Griessbach S.,

636   Vernier J-P., and Tilmes S., The role of tropical volcanic eruptions in exacerbating

637   Indian droughts, Sci. Rep., 11, 2714, doi.org/10.1038/s41598-021-81566-0, 2021b.

638   Gogoi, M. M., Tandule, C. R., Jayachandran, V., Kompalli, S. K., Nair, V. S., Gopal, K. R.

639   and Babu, S. S.: Spatial gradient of aerosol mass concentrations and size distributions

640   over southeastern Arabian Sea and equatorial Indian Ocean during ICARB-2018,

641   Atmos. Environ., 213, 727–738, doi:10.1016/j.atmosenv.2019.06.038, 2019.

642   Jose, S., Nair, V. S. and Babu, S. S.: Anthropogenic emissions from South Asia reverses the

643   aerosol indirect effect over the northern Indian Ocean, Sci. Rep., 10, 18360,

644   doi:10.1038/s41598-020-74897-x, 2020.

645   Karambelas, A., Holloway, T., Kinney, P. L., Fiore, A. M., Defries, R., Kiesewetter, G. and

646   Heyes, C.: Urban versus rural health impacts attributable to PM2.5 and O3 in northern

647   India, Environ. Res. Lett., 13, 064010, doi:10.1088/1748-9326/aac24d, 2018.

648   Lu, Z., Zhang, Q. and Streets, D. G.: Sulfur dioxide and primary carbonaceous aerosol

649   emissions in China and India, 1996-2010, Atmos. Chem. Phys., 11, 9839–9864,

650   doi:10.5194/acp-11-9839-2011, 2011.

651   Mahowald, N. M., Hamilton, D. S., Mackey, K. R. M., Moore, J. K., Baker, A. R., Scanza, R.

652   A. and Zhang, Y.: Aerosol trace metal leaching and impacts on marine microorganisms,

653   Nat. Commun., 9, 2614, doi:10.1038/s41467-018-04970-7, 2018.

654   Mhawish, A. T., Banerjee, M., Sorek-Hamer, A., Lyapustin, D., Broday, and Chatfield, R.:

655   Comparison and Evaluation of MODIS Multi-Angle Implementation of Atmospheric

656   Correction (MAIAC) Aerosol Product over South Asia, Remote Sens. of Environ., 224,

657   12–28, 2019.

658   Mayol-Bracero, O. L., Gabriel, R., Andreae, M. O., Kirchstetter, T. W., Novakov, T., Ogren,

659   J., Sheridan, P. and Streets, D. G.: Carbonaceous aerosols over the Indian Ocean during

660   the Indian Ocean Experiment (INDOEX): Chemical characterization, optical properties,

661   and probable sources, J. Geophys. Res. Atmos., 107, 8030,

662   doi:10.1029/2000JD000039, 2002.

663   McFarquhar, G. M. and Wang, H.: Effects of aerosols on trade wind cumuli over the Indian

664   Ocean: Model simulations, Q. J. R. Meteorol. Soc., 132, 821–843,

665   doi:10.1256/qj.04.179, 2006.

666   Meehl, G. A., Arblaster, J. M. and Collins, W. D.: Effects of black carbon aerosols on the

667   Indian monsoon, J. Clim., 21, 2869–2882, doi:10.1175/2007JCLI1777.1, 2008.

668   Nair, V. S., Babu, S. S., Manoj, M. R., Moorthy, K. K. and Chin, M.: Direct radiative effects

669   of aerosols over South Asia from observations and modeling, Clim. Dyn., 49, 1411–

670   1428, doi:10.1007/s00382-016-3384-0, 2017.

671   Neubauer, D., Lohmann, U., Hoose, C. and Frontoso, M. G.: Impact of the representation of

672   marine stratocumulus clouds on the anthropogenic aerosol effect, Atmos. Chem. Phys.,

673   14, 11997–12022, doi:10.5194/acp-14-11997-2014, 2014.

674   Paliwal, U., Sharma, M. and Burkhart, J. F.: Monthly and spatially resolved black carbon

675   emission inventory of India: Uncertainty analysis, Atmos. Chem. Phys., 16, 12457–

676   12476, doi:10.5194/acp-16-12457-2016, 2016.

677   Papaspiropoulos, G., Martinsson, B. G., Zahn, A., Brenninkmeijer, C. A. M., Hermann, M.,

678   Heintzenberg, J., Fischer, H. and Van Velthoven, P. F. J.: Aerosol elemental

679   concentrations in the tropopause region from intercontinental flights with the Civil

680   Aircraft for Regular Investigation of the Atmosphere Based on an Instrument Container

681   (CARIBIC) platform, J. Geophys. Res. Atmos., 107, 4671, doi:10.1029/2002JD002344,

682   2002.

683   Pathak, H. S., Satheesh, S. K., Moorthy, K. K. and Nanjundiah, R. S.: Assessment of regional

684   aerosol radiative effects under the SWAAMI campaign - Part 2: Clear-sky direct

685   shortwave radiative forcing using multi-year assimilated data over the Indian

686   subcontinent, Atmos. Chem. Phys., 20, 14237–14252, doi:10.5194/acp-20-14237-2020,

687   2020.

688   Penner, J. E., Chuang, C. C. and Grant, K.: Climate forcing by carbonaceous and sulfate

689   aerosols, Clim. Dyn., 14, 839–851, doi:10.1007/s003820050259, 1998.

690   Rajeev, K. and Ramanathan, V.: Direct observations of clear-sky aerosol radiative forcing

691   from space during the Indian Ocean Experiment, J. Geophys. Res. Atmos., 106, 17221–

692   17235, doi:10.1029/2000JD900723, 2001.

693   Ramachandran, S., Rupakheti, M. and Lawrence, M. G.: Aerosol-induced atmospheric

694   heating rate decreases over South and East Asia as a result of changing content and

695   composition, Sci. Rep., 10, 20091, doi:10.1038/s41598-020-76936-z, 2020a.

696   Ramachandran, S., Rupakheti, M. and Lawrence, M. G.: Black carbon dominates the aerosol

697   absorption over the Indo-Gangetic Plain and the Himalayan foothills, Environ. Int.,

698   142, 105814, doi:10.1016/j.envint.2020.105814, 2020b.

699   Ramanathan, V., Chung, C., Kim, D., Bettge, T., Buja, L., Kiehl, J. T., Washington, W. M.,

700   Fu, Q., Sikka, D. R. and Wild, M.: Atmospheric brown clouds: Impacts on South Asian

701   climate and hydrological cycle, Proc. Natl. Acad. Sci. U. S. A., 102, 5326–5333,

702   doi:10.1073/pnas.0500656102, 2005.

703   Ramanathan, V., Crutzen, P. J., Lelieveld, J., Mitra, A. P., Althausen, D., Anderson, J.,

704   Andreae, M. O., Cantrell, W., Cass, G. R., Chung, C. E., Clarke, A. D., Coakley, J. A.,

705   Collins, W. D., Conant, W. C., Dulac, F., Heintzenberg, J., Heymsfield, A. J., Holben,

706   B., Howell, S., Hudson, J., Jayaraman, A., Kiehl, J. T., Krishnamurti, T. N., Lubin, D.,

707   McFarquhar, G., Novakov, T., Ogren, J. A., Podgorny, I. A., Prather, K., Priestley, K.,

708   Prospero, J. M., Quinn, P. K., Rajeev, K., Rasch, P., Rupert, S., Sadourny, R., Satheesh,

709   S. K., Shaw, G. E., Sheridan, P. and Valero, F. P. J.: Indian Ocean Experiment: An

710   integrated analysis of the climate forcing and effects of the great Indo-Asian haze, J.

711   Geophys. Res. Atmos., 106, 28371–28398, doi:10.1029/2001JD900133, 2001.

712   Randel, W. J., Park, M., Emmons, L., Kinnison, D., Bernath, P., Walker, K. A., Boone, C.

713   and Pumphrey, H.: Asian monsoon transport of pollution to the stratosphere, Science,

714   328, 611–613, doi:10.1126/science.1182274, 2010

715   Reddy, M. S., Boucher, O., Venkataraman, C., Verma, S., Léon, J. F., Bellouin, N. and Pham,

716   M.: General circulation model estimates of aerosol transport and radiative forcing

717   during the Indian Ocean Experiment, J. Geophys. Res., 109, D16205,

718   doi:10.1029/2004JD004557, 2004.

719   Robrecht, S., Vogel, B., Grooß, J.-U., Rosenlof, K., Thornberry, T., Rollins, A., Krämer, M.,

720   Christensen, L. and Müller, R.: Mechanism of ozone loss under enhanced water vapour

721   conditions in the mid-latitude lower stratosphere in summer, Atmos. Chem. Phys., 19,

722   5805–5833, doi:10.5194/acp-19-5805-2019, 2019.

723   Romatschke, U. and Houze, R. A.: Characteristics of precipitating convective systems in the

724   South Asian monsoon, J. Hydrometeorol., 12, 3–26, doi:10.1175/2010JHM1289.1,

725   2011.

726   Satheesh, S. K., Ramanathan, V., Holben, B. N., Krishna Moorthy, K., Loeb, N. G., Mating,

727   H., Prospero, J. M. and Savoie, D.: Chemical, microphysical, and radiative effects of

728   Indian Ocean aerosols, J. Geophys. Res., 107, 4725, doi:10.1029/2002JD002463, 2002.

729   Satheesh, S. K. and Ramanathan, V.: Large differences in tropical aerosol forcing at the top

730   of the atmosphere and Earth's surface, Nature, 405, 60–63, doi:10.1038/35011039,

731   2000.

732   Shindell, D. T.: Climate and ozone response to increased stratospheric water vapor, Geophys.

733   Res. Lett., 28, 1551–1554, doi:10.1029/ 1999GL011197, 2001.

734   Solomon, S., Rosenlof, K. H., Portmann, R. W., Daniel, J. S., Davis, S. M., Sanford, T. J. and

735   Plattner G. K.: Contributions of stratospheric water vapor to decadal changes in the rate

736   of global warming, Science, 327, 1219–1223, 0.1126/science.1182488, 2010.

737   Stier, P., Feichter, J., Kinne, S., Kloster, S., Vignati, E., Wilson, J., Ganzeveld, L., Tegen, I.,

738   Werner, M., Balkanski, Y., Schulz, M., Boucher, O., Minikin, A., and Petzold, A.: The

739   aerosol-climate model ECHAM5-HAM, Atmos. Chem. Phys., 5, 1125–1156,

740   doi:10.5194/acp-5-1125-2005, 2005.

741   Taylor, K. E., Williamson, D. L. and Zwiers, F. W.: The Sea Surface Temperature and Sea-

742   Ice Concentration Boundary Conditions for AMIP II Simulations, Program for Climate

743   Model Diagnosis and Intercomparison (PCMDI), Lawrence Livermore Natl. Lab.

744   Livermore, Calif., Rep., 60, 1–28 http://www-pcmdi.llnl.gov/publications/ab60.html,

745   2000.

746   Tegen, I., Neubauer, D., Ferrachat, S., Drian, C. S. Le, Bey, I., Schutgens, N., Stier, P.,

747   Watson-Parris, D., Stanelle, T., Schmidt, H., Rast, S., Kokkola, H., Schultz, M.,

748   Schroeder, S., Daskalakis, N., Barthel, S., Heinold, B. and Lohmann, U.: The global

749   aerosol-climate model echam6.3-ham2.3 -Part 1: Aerosol evaluation, Geosci. Model

750   Dev., 12, 1643–1677, doi:10.5194/gmd-12-1643-2019, 2019.

751   Tegen, I., Harrison, S. P., Kohfeld, K. E., Prentice, I. C., Coe, M., and Heimann, M.: Impact

752   of vegetation and preferential source areas on global dust aerosol: Results from a model

753   study, J. Geophys. Res.-Atmos., 107, 14–27, https://doi.org/10.1029/2001JD000963,

754   2002.

755   Yue, J., Russell, J., Gan, Q., Wang, T., Rong, P., Garcia, R. and Mlynczak, M.: Increasing

756   Water Vapor in the Stratosphere and Mesosphere After 2002, Geophys. Res. Lett., 46,

757   13452–13460, doi:10.1029/2019GL084973, 2019.

758   Zhang, K., O'Donnell, D., Kazil, J., Stier, P., Kinne, S., Lohmann, U., Ferrachat, S., Croft,

759   B., Quaas, J., Wan, H., Rast, S. and Feichter, J.: The global aerosol-climate model

760   ECHAM-HAM, version 2: Sensitivity to improvements in process representations,

761   Atmos. Chem. Phys., 12, 8911–8949, doi:10.5194/acp-12-8911-2012, 2012.